UC Office of the President
Recent Work

Title

Proliferation tracing with single-cell mass cytometry optimizes generation of stem cell memory-like T cells.

Permalink

Journal

ISSN

Authors

Good, Zinaida
Borges, Luciene
Vivanco Gonzalez, Nora
et al.

Publication Date

DOI

Peer reviewed

Proliferative tracing with single-cell mass cytometry optimizes generation of stem cell memory-like T cells

Zinaida Good[1,2,3,4,8], **Luciene Borges**[4,*], **Nora Vivanco Gonzalez**[1,4,*], **Bita Sahaf**[5], **Nikolay Samusik**[2,3], **Robert Tibshirani**[6,7], **Garry P. Nolan**[2,3,8,§], and **Sean C. Bendall**[4,8,§,†]

[1]PhD Program in Immunology, Stanford University, Stanford, CA 94305, USA.

[2]Baxter Laboratory in Stem Cell Biology, Stanford University, Stanford, CA 94305, USA.

[3]Department of Microbiology and Immunology, Stanford University, Stanford, CA 94305, USA.

[4]Department of Pathology, Stanford University, Stanford, CA 94305, USA.

[5]Cancer Institute, Department of Medicine, Stanford University, Stanford, CA 94305, USA.

[6]Department of Statistics, and Stanford University, Stanford, CA 94305, USA.

[7]Department of Health Research and Policy, Stanford University, Stanford, CA 94305, USA.

[8]Parker Institute for Cancer Immunotherapy.

Abstract

Selective differentiation of naïve T lymphocytes into multipotent T cells is of great interest clinically for the generation of cell-based cancer immunotherapies. Cellular differentiation depends crucially on division state and time. Here we adapt a dye-dilution assay for tracking cell proliferative history to mass cytometry, and uncouple division, time and regulatory protein expression in single naïve human T cells during their activation and expansion in a complex *ex vivo* milieu. Using 23 markers, we defined groups of proteins that are controlled predominantly by division state or time, and found that undivided cells account for the majority of phenotypic diversity. We next built a map of cell state changes during naïve T-cell expansion. By examining cell signaling on this map, we rationally selected ibrutinib, a BTK/ITK inhibitor administered before activation, to direct differentiation toward a T_{SCM}-like phenotype. This method for tracing cell fate across division states and time can be broadly applied for directing cellular differentiation.

Author Manuscript

Cellular differentiation is a continuous and coordinated process that integrates cell-intrinsic and extrinsic signals, leading to changes in phenotype, proliferation, and death. The linkage of cell division with time during differentiation, especially in human cell systems, remains elusive. Multiple cellular processes have been implicated in T-cell fate selection during an immune response, including asymmetric distribution of polarity proteins during initial division[1] and the varying 'built-in' capabilities of individual antigen-specific T cells[2, 3], but the relative contributions of these two processes to T-cell fate selection are not well defined[4]. Moreover, comparison of time-dependent and division state-dependent changes to our knowledge has not yet been performed in any cell context. An improved model of early T-cell fate choices across time and divisions will help clarify the mechanistic underpinnings and serve as a guide in T-cell engineering efforts for clinical applications.

Mapping differentiation across time and division states in complex cellular systems requires simultaneous high-throughput measurements of phenotype, function and proliferative history in single cells across multiple timepoints. Despite advances in sequencing-based techniques for lineage tracing[5], a compatible method for measuring proliferative history is unavailable, whereas spectral overlap in flow cytometry-based methods[6] precludes high-dimensional cell phenotyping across divisions. Cytometry by time-of-flight (CyTOF; mass cytometry)[7] is a powerful technique for high-throughput proteomic monitoring of single-cell phenotypes, but cannot yet track proliferative history. Starting with a fluorescent dye dilution approach[8, 9], we have created a mass cytometry assay, where the proliferative history of single cells across 0-7 divisions can be traced in complex cell mixtures, while performing highly multiplexed single-cell analyses for function and phenotype.

This approach enabled understanding of primary T-cell differentiation in the context of expansion for cancer immunotherapy[10], and computationally uncoupling time in culture from cell division state. By examining cell signaling on a map of cell state transitions, we selected treatment with a small molecule ibrutinib prior to expansion, to skew early naïve T-cell differentiation towards a subset resembling clinically desirable T stem cell memory (T_{SCM}) cells[11, 12].

Fluorescent dye dilution assays[6], originally developed for T cells[8], are useful for counting cell divisions by flow cytometry. To adapt carboxyfluorescein succinimidyl ester (CFSE) dilution assay[8, 9] to mass cytometry, we leveraged the structural similarity between CFSE and fluorescein isothiocyanate (FITC) to track changes in CFSE signal via a metal-labeled anti-FITC antibody (Fig. 1a). Dividing cells pass ~50% of CFSE to each daughter cell, providing a proxy for counting cell divisions.

With optimal CFSE detection conditions for mass cytometry (Supplementary Data 1), we confirmed non-toxic, homogeneous labeling of primary human CD8+ T cells with 80 μM CFSE in the presence of serum[6] (*data not shown*). In contrast to anti-FITC monoclonal antibodies, a polyclonal produced a strong and specific signal (Fig. 1b, Supplementary Figs. 1a-e). Here, flow cytometry and mass cytometry yielded an equivalent CFSE signal (Fig. 1c), with minimal background for mass cytometry, as is typical[7]. Lack of autofluorescence

enabled us to detect an equivalent CFSE signal in other cell types, such as monocytes and dendritic cells (Supplementary Fig. 1f).

To test this method in resolving division states, we followed T-cell proliferation during *ex vivo* expansion for cancer immunotherapy[13]. We selected the rapid expansion protocol (REP)[10] as a model system (Fig. 1d), where we discerned the CFSE-traced T cells from the unlabeled accessory cells and distinguished ≥5 cell divisions (Fig. 1e). Using mathematical modeling based on local regression, we assigned division IDs to all cells falling into the ≥80% confidence region. The percentage of cells assigned to each division was nearly identical for samples analyzed by flow and mass cytometry (Spearman's rank correlation coefficient: 0.978; Fig. 1f). Correlation in CFSE signal was also high for these samples (Spearman's rank correlation coefficient: 0.997; Supplementary Fig. 2a). To estimate loss of signal without division, we applied linear regression to cells falling into the same division over multiple days. If drifts were the same for flow and mass cytometry, we would expect the slope to be 1. We observed that this slope was consistently lower than 1 (division IDs 0-7: mean ± s.d. = 0.496 ± 0.161; Supplementary Fig. 2b), suggesting that CFSE fluorescence is less stable than the CFSE epitopes detected in mass cytometry. As expected, CFSE signal decreased ~50% each time cells divided, irrespective of the method used (Fig. 1g) or timepoint assessed (Supplementary Fig. 2c).

With a panel of T-cell receptors relevant to immunotherapy and T-cell fate specification[11, 12] (Supplementary Data 2-6), we reconciled early steps in naïve CD8^{+} T-cell differentiation in REP. Although expression of a few proteins across divisions has previously been analyzed by flow cytometry[14], a high-dimensional analysis has not been performed. We tracked division state- and time-dependent dynamics of 23 markers after using 13 parameters for stringent selection of CFSE^{+} CD8^{+} T cells (DNA, size, viability, apoptotic status, lineage; Supplementary Data 2, Supplementary Fig. 3) and additional parameters for data quality (*i.e.* normalization, barcoding). Tracking individual protein expression in CD8^{+} T cells from the naïve resting state showed that expression of some markers changed dramatically as cells divided (Supplementary Fig. 4). For example, CD69[Low] T cells, which may be mistaken for poorly activated, had in fact divided the most, whereas regulatory protein expression (*e.g.* LAG3 and BTLA) remained consistent across divisions.

To computationally disentangle division state-dependent from time-dependent changes, we normalized average marker expression to either division 0 for each day, or the earliest timepoint for each division (Fig. 2a). Here, division state-dependent changes, especially upregulation, were more pronounced than time-dependent changes in early T-cell differentiation during *ex vivo* expansion (Fig. 2b). Moreover, time-dependent changes were distinct from division state-dependent changes. For example, expression of the activation molecule CD69 decreased with division at each timepoint, yet changed little within each division over time. A multivariate regression model quantified the relative effects of division and time on levels of each regulatory protein (Fig. 2c). The strongest division state-dependent effect was the switch from CD45RA to CD45RO isoform, an important event in T-cell memory specification. In contrast, reduced phosphorylation of ribosomal protein S6 (pRPS6), downstream of mTOR, was significantly time-dependent. Besides the expected connection between differentiation and time, the consistency and magnitude of division

state-dependent changes indicate a fundamental link between proliferation and differentiation of naïve CD8^{+} T cells in this expansion setting.

Surprisingly, analysis of division state- and time-dependent changes revealed that phenotypic diversity, estimated by standard deviation (s.d.) in individual protein expression, decreased consistently in a division-, but not time-dependent manner for the majority of molecules examined (Supplementary Fig. 5). This, together with the link between differentiation and proliferation, prompted us to leverage the high-dimensional single-cell data to broadly map naïve CD8^{+} T-cell differentiation across division states.

To visualize high-dimensional single-cell data, we built force-directed graphs[15] using *Vortex* software[16]. The resulting maps aid visualizing *continuous* processes, such as cellular differentiation[15]. Here, edges hold cells together with constant spring-like forces, while repulsion is mediated by forces proportional to cell dissimilarity in multidimensional protein expression[15, 16]. These repulsive and attractive forces eventually converge to a balanced state, where similar cells are located near each other, and dissimilar cells are far apart (this is not always the case in *t*SNE plots). We modified *Vortex* to only allow edge connections either between consecutive timepoints, as in the *FLOW-MAP* algorithm[17], or between subsequent divisions to take advantage of our proliferative history data. This feature is now publicly available in *Vortex*. The single-cell phenotypic maps presented here connect cells only within neighboring division states (−1, 0, +1).

We initially focused on day 3, when the majority of cells were in divisions 0 or 1 (Fig. 3a). At this early time in naïve CD8^{+} T-cell differentiation, undivided cells unexpectedly occupied the majority of phenotypic niches (dark green nodes, Fig. 3b). Partial cell activation is unlikely to contribute to this undivided cell diversity, since 99.2% of undivided cells in this culture were CD69[High] (Supplementary Fig. 4b). We annotated this phenotypic map based on all single-cell markers quantified (Supplementary Fig. 6). To understand how cells advanced through phenotypic space, we applied diffusion maps[18]. This approach identifies the most likely sequence of cell state transitions, a metric called diffusion pseudo-time (DPT; Supplementary Fig. 7). Overlaying DPT onto our map exposed a continuum of phenotypes from the least differentiated to the two most differentiated states (Fig. 3c), which overlapped with 3 prominent regions in Fig. 3b. Importantly, undivided cells had the highest DPT diversity (estimated by s.d.) and completely covered the range of DPT values (Fig. 3d). Using lasso[19], we found that CD25 and CD137 had the highest coefficients for predicting DPT1 and DPT2, respectively (Supplementary Data 7). This finding was corroborated by a correlation analysis (Supplementary Data 7).

As an independent metric of high-dimensional cellular diversity, we calculated angular distance to an average cell within each division (Fig. 3e). This metric confirmed that undivided cells had the highest phenotypic diversity, and phenotypic diversity significantly decreased with successive divisions (Fig. 3f). This observation held true on subsequent days (Fig. 3g and Supplementary Fig. 8).

To obtain an orthogonal view of diversity during early differentiation of naïve CD8^{+} T cells without a priori target bias, we performed droplet-based single-cell RNA-sequencing

(scRNA-seq) on CD8^{+} T cells prospectively isolated from divisions 0, 1, or 2 on day 3 of REP (Fig. 3h and Supplementary Fig 9). We then selected the 1,000 most variably expressed genes to construct a force-directed graph, which provided insight into biological identity of genes underlying cellular diversity (Fig. 3i and Supplementary Figs. 9-11). Undivided cells again occupied the majority of phenotypic niches and had a significantly higher phenotypic diversity than cells that divided either once or twice (Fig. 3j and Supplementary Fig. 12). Together, these data confirm that undivided CD8^{+} T cells display the largest phenotypic diversity in our system.

By day 7 of differentiation, naïve CD8^{+} T cells expanded into new phenotypic niches and converged onto two main subpopulations (Figs. 4a,b; Supplementary Figs. 13-15), which resembled T_{SCM} and dysfunctional cells. T_{SCM} are minimally differentiated antigen-experienced T cells that are clinically favorable for immunotherapy due to their excellent engraftment, persistence, and multifunctionality[11, 12]. Clinically undesirable dysfunctional T cells express ≥2 inhibitory receptors and have poor proliferative capacity and effector functions[11]. Here, we defined T_{SCM}-like cells as antigen-experienced (divided following TCR engagement) CD45RA[High] CD45RO[Low] CD27[High] CD127[High] CCR7[High] CTLA4[Low] LAG3[Low] PD1[Low] CD57[Low], and dysfunctional-phenotype cells as antigen-experienced CD27[Low] PD1[High] LAG3[High] CTLA4[High][11, 12, 20]. Relative to T_{SCM}-like cells, dysfunctional-phenotype cells were CD45RA[Low] CD45RO[High] CD5[Low] CD7[Low] CD25[High] CD27[Low] CD52[Low] CD69[High] CCR7[Low] and contained a subpopulation expressing CD57 senescence marker[11]. Since T_{SCM} cells are similar to naïve T cells in their protein expression[12], allowing connections only among cells in consecutive division states ensured that true division history defined cell locations in the final force-directed map. This map allowed us to devise a simple fluorescence-activated cell sorting (FACS) scheme to prospectively isolate and test functional properties of T_{SCM}-like and dysfunctional-phenotype subsets (Fig. 4a, *right* and Supplementary Fig. 16). Upon re-stimulation, T_{SCM}-like cells were superior in their proliferative potential, resistance to apoptosis, and reduced dysfunctional marker expression. Using intracellular staining, we confirmed that T_{SCM}-like cells produced more IL-2 and less IFN-γ and TNF-α (Supplementary Fig. 17), as expected for T_{SCM}-enriched cells[21].

DPT analysis confirmed the minimally differentiated state of T_{SCM}-like cells as DPT[Low] (Fig. 4b and Supplementary Fig. 13). Interestingly, DPT correlated to pRPS6 that indicates mTOR pathway activity (Figs. 4a,b; Supplementary Figs. 13-15; Supplementary Data 7). The DPT-pRPS6 correlation remained irrespective of division state (Supplementary Fig. 18, *black box*), but pRPS6 decreased the most with time (Fig. 3c). These findings, together with high undivided cell diversity, led us to hypothesize that blocking signaling upstream of pRPS6 prior to the first division would direct naïve T-cell differentiation towards the minimally differentiated (DPT[Low]) T_{SCM}-like fate (Fig. 4a). To test this, we selected inhibitors of the mTOR pathway (rapamycin), or the upstream TCR signaling pathway (ibrutinib, a dual BTK/ITK inhibitor, which inhibits ITK downstream of TCR[22]) and administered them at a higher concentration during the initial activation (days 0-2) than the high proliferative phase (days 3-7). We found that ibrutinib skewed T-cell differentiation away from the pRPS6[High] path and towards the pRPS6[Low] path ending at the T_{SCM}-like state (Figs. 4b,c; Supplementary Figs. 15,19; Supplementary Data 8). At the concentration

tested, rapamycin reduced overall proliferation and hindered differentiation by locking T cells in a naïve-like CD127^{++} state (Supplementary Figs. 19-20; Supplementary Data 8). Thus, early tuning of TCR or mTOR signaling had pronounced effects on phenotypic output.

Mechanistically, ibrutinib affected differentiation early in time and division. Namely, on day 3 all divisions had significantly lower DPT (Supplementary Fig. 19c) and were closer to the T$_{SCM}$-like state than vehicle-treated cells (Supplementary Fig. 21). Delaying ibrutinib treatment until day 3 reduced the fate skewing effect (Supplementary Fig. 22). Ibrutinib reduced apoptosis and cell death in both pRPS6^{+} and pRPS6^{-} compartments (Supplementary Data 8), arguing for re-directing of naïve-derived CD8^{+} cells towards the T$_{SCM}$-like differentiation endpoint and against drug-induced subset selection.

T$_{SCM}$ subset enrichment in chimeric antigen receptor (CAR)-engineered T cells enhances intracellular production of IL-2, but not of effector cytokines IFN-γ and TNF-α, when examined in bulk[21]. Similarly, ibrutinib enrichment of T$_{SCM}$-like subset improved intracellular production of IL-2, but not of IFN-γ and TNF-α, in bulk CD8^{+} T cells (Supplementary Fig. 23). As expected[21], the benefit of T$_{SCM}$ enrichment was the increased IFN-γ and TNF-α production by effector T cells generated in presence of ibrutinib (Supplementary Fig. 24). Adding ibrutinib only prior to day 3 was sufficient to partially skew cells towards T$_{SCM}$-like fate, and superior to both vehicle and continuous ibrutinib treatment in enhancing intracellular IL-2 and IFN-γ production by bulk CD8^{+} T cells (Supplementary Figs. 23- 25).

Uncoupling the sequence of cellular transitions through phenotypic space in the context of time and division states is essential for creating better models of cellular differentiation. Here, we present a method for simultaneously tracing the proliferative history and phenotype of chemically labeled cells using highly multiplexed single-cell mass cytometry. While applied to primary human T cells here, we believe that this approach is generally applicable to tracing cell fate in complex mixtures for a variety of primary samples and cell lines[23], as well as to transplantation animal models where input material or genetic tracing could be limited.

We found that early differentiation of naïve CD8^{+} T cells during expansion for immunotherapy is linked to division state. Using a comprehensive panel of T-cell specialization and exhaustion markers, we established that undivided cells had the highest phenotypic diversity. Unbiased scRNA-seq confirmed this observation and identified gene expression programs driving diversity. While we uncovered some mechanisms that linked division state and early cell fate choices, we did not investigate how cells acquired diverse phenotypes without division. Possibilities include the intrinsic predisposition of clonally-derived naïve T cells to produce diverse proportions of effector and memory populations[2, 3], differences in TCR signaling, and co-receptor engagement[24,25]. Our results do not contradict asymmetric division, which plays a role in T-cell fate[1, 4]

The origin of T$_{SCM}$ cells is currently of great interest[12]. While did not trace fate of individual cells over time, our data suggest that in the context of REP, T$_{SCM}$-like cells arise from a CD45RA^{High} subpopulation with low pRPS6 signaling. These cells are CD25^{Low},

indicating that our data are consistent with observations that $CD25^{High}$ $CD8^+$ T cells give rise to terminally differentiated and short-lived effector cells, whereas $CD25^{Low}$ cells eventually give rise to functional long-lived memory cells[26]. True T_{SCM} and dysfunctional states are more distant and not fully represented in REP[10], our model system that was not design to mimic normal T-cell differentiation processes. Further studies on the mechanisms linking proliferation to differentiation *in vivo* could benefit from this method.

We believe that our approach of identifying optimal intervention strategies based on high-resolution maps of normal cellular differentiation will be broadly applicable to guiding fate of endogenous or engineered T lymphocytes in cancer immunotherapy (Fig. 4d). Here, we selected ibrutinib to direct naïve T-cell fate towards the T_{SCM}-like state. While ibrutinib reduced pRPS6 signaling and enhanced the expansion into our T_{SCM}-like cell compartment, we cannot rule out indirect effects of the inhibitor on antigen-presenting cells. In the future, ibrutinib could be useful for directing tumor-infiltrating T lymphocytes or CAR T cells towards T_{SCM} or other desired fate, which is an important direction in cancer immunotherapy research[12,21]. Our results may also help explain the recently observed T_{SCM} expansion in patients with chronic lymphocytic leukemia (CLL) receiving ibrutinib[27], as well as the improvement in CAR T efficacy when administered after or with ibrutinib for treatment of CLL in the clinic[28-30].

In conclusion, this framework for tracing and directing the fate of labeled T cells should be broadly useful in stem cell biology and hematology and for improving clinical outcomes in cancer immunotherapy.

Online Methods

Cells

De-identified human blood was obtained from healthy adult donors under informed consent (Stanford Blood Center, Palo Alto, CA). Use of these samples was approved by Stanford's Institutional Review Board. Peripheral blood mononuclear cells (PBMCs) were isolated from Trima Accel leukocyte reduction system (LRS) chambers (Terumo BCT, Lakewood, CO) using Ficoll-Paque Plus (GE Healthcare, Chicago, IL, USA) density gradient centrifugation according to manufacturer's instructions. For long-term storage, PBMCs were resuspended in FBS with 10% DMSO and stored in liquid nitrogen at density $1\text{-}5\times10^7$ cells/mL.

Cryopreserved PBMCs were thawed into cell culture medium (CCM; RPMI 1640 containing 10% FBS, 1x L-glutamine, and 1x penicillin/streptomycin; Thermo Fisher Scientific Waltham, MA, USA) supplemented with 25 U/mL benzonase (Sigma-Aldrich, St. Louis, MO, USA). Cells were then pelleted for 5 min at 250 g, resuspended in 10 mL CCM, rested at 37°C, 5% CO_2 for 60 minutes, filtered through a 40 μm strainer, and counted. Where indicated, naïve T cells were enriched using Naïve Pan T Cell Isolation Kit (Miltenyi Biotec #130-097-095, Bergisch Gladbach, Germany) according to manufacturer's instructions.

CFSE labeling

Unless otherwise noted, carboxyfluorescein succinimidyl ester (CFSE) labeling was performed as described by Quah and Parish[6, 31]. Briefly, 50 μg carboxyfluorescein diacetate succinimidyl ester (CFDA-SE) was reconstituted in 18 μL DMSO (CellTrace CFSE Cell Proliferation Kit, Thermo Fisher Scientific #C34554) to create a 5 mM stock immediately prior to labeling. Cells were resuspended in 1 mL warm CCM and transferred into a new 15 mL Falcon tube lying horizontally. A drop containing 110 μL warm PBS was placed on a side of the tube, and 17.6 μL of 5 mM CFDA-SE was diluted into the drop. The tube was then quickly capped and turned upside right while being vortexed gently, yielding a final concentration of 80 μM CFDA-SE. Cells were incubated for 5 minutes at room temperature, quenched by adding 9 mL warm CCM, and washed twice with 10 mL warm CCM. When only naïve T cells were labeled with CFSE, they were combined with the CFSE-negative PBMC fraction devoid of naïve T cells after labeling to restore original cell proportions. All centrifuging steps for live cells were done for 5 minutes at 250 g, room temperature. CFSE and labeled cells were protected from light throughout the experiment.

During protocol optimization, we tested the above labeling protocol for $0.1\text{-}10\times10^7$ cells and CFSE concentrations in range of 0.2 μM to 320 μM. We assessed long-term cell viability and proliferation. We also tested manufacturer's labeling protocol for CFSE concentrations 0.2 μM to 20 μM, as well as other CFSE suppliers (Biolegend #422701, San Diego, CA, USA).

Expansion and treatment of primary human T cells

T cells were induced to proliferate using the rapid expansion protocol (REP) for adoptive transfer therapies[10]. Briefly, ~40×10^6 cells were plated into a well of a 24-well plate with 2 mL CCM and 600 ng anti-CD3ε antibody (clone OKT3, Biolegend #317304). Where indicated, cells were pre-treated with vehicle (DMSO), ibrutinib (PCI-32765; Cellagen Technology #C7327, San Diego, CA, USA; 700 ng/mL or 1.59 μM), or rapamycin (Cell Signaling Technology #9904S, Danvers, MA, USA; 50 ng/mL or 54.70 nM) for 30 minutes. Starting at 48 hours post-activation, cells were maintained at ~2×10^6 cells/mL in CCM containing 300 ng/mL anti-CD3ε antibody and 50 U/mL (5 ng/mL) recombinant human IL-2 (PeproTech #200-02, Rocky Hill, NJ, USA) and relevant concentrations of chemical inhibitors (ibrutinib: 700 ng/mL or 1.59 μM on days 0-2, and physiological concentrations[32, 33] of 140 ng/mL or 318 nM on days 3-7; rapamycin: 50 ng/mL or 54.70 nM on days 0-2, and physiological concentrations[34, 35] of 10 ng/mL or 10.94 nM on days 3-7). Where indicated, ibrutinib was only added on either days 0-2 or days 3-7, with vehicle on the remaining days. In initial experiments, we tested a lower concentration of ibrutinib (140 ng/mL on days 0-7; skewing effect was reduced; data not shown) and a higher concentration of ibrutinib (7 μg/mL on days 0-2, 1.4 μg/mL on days 3-7; we observed cell death and no proliferation; data not shown) prior to selecting the above ibrutinib treatment regimen. Samples containing 30% of cells from each condition were collected on days 0, 3, 4, 5, and 7, then fixed and stored at −80°C for analyses by flow cytometry and mass cytometry.

Analysis of T$_{SCM}$-like and increased dysfunction subsets

To compare the abilities of putative T$_{SCM}$-like and dysfunctional cells to proliferate, persist, and maintain beneficial phenotype, naïve CFSE$^+$ T cells were cultured using REP for 7 days to form these subsets. Based on the observed pattern of protein expression by day 7 (Supplementary Figs. 13-14), we defined a FACS staining panel and gating strategy (Supplementary Fig. 16b). Fc receptors were blocked using Human TruStain FcX (Biolegend #422302) following manufacturer's instructions. Surface antibody staining was performed with anti-CD3ε-V500 (clone UCHT1, BD Biosciences #561416, Franklin Lakes, NJ, USA), anti-CD8α-PerCP (clone SK1, BD Biosciences #347314), anti-CD27-PE-Cy7 (clone O323, Biolegend #302837), anti-CD45RA-AlexaFluor700 (clone HI100, Biolegend #304119), and anti-CD279-PE (PD1; clone EH12.2H7, Biolegend #329905) antibodies for 30 minutes on ice in FACS buffer (PBS with 2% human serum and 2 mM EDTA). Cells were then washed once with FACS buffer and stained with 7-AAD (Biolegend #420404) to exclude dead cells following manufacturer's instructions. Next, cells were resuspended in FACS buffer to sort out putative T$_{SCM}$ and dysfunctional subsets on FACS Aria II (BD Biosciences). The post-sort purity of each subset was >90%.

To assess the functional properties of the putative T$_{SCM}$-like and dysfunctional subsets, we re-labeled the sorted cells with CFSE and cultured with new autologous CFSE-negative accessory cells using REP for 3 days (Supplementary Fig. 16a). To quantify the percentage of cells in S phase, the culture medium was supplemented with 100 μM 5-iodo-2'-deoxyuridine (IdU; Sigma-Aldrich #I7125-5G) 30 minutes prior to sample collection.

Intracellular cytokine production

To assess intracellular production of IL-2, IFN-γ, and TNF-α at the indicated collection timepoints, cells were resuspended cells 10^6 per mL and stimulated with 50 ng/mL phorbol 12-myristate 13-acetate (PMA; Sigma-Aldrich #P8139, dissolved in ethanol) and 500 ng/mL ionomycin (Sigma-Aldrich #I0634, dissolved in ethanol) in presence of 1x Brefeldin A (Biolegend #420601) for 4 hours. Cells were stained using an antibody panel in Supplementary Data 5 and assessed by mass cytometry.

Mass cytometry

Samples were processed as previously described[7]. To stain cells for viability, cisplatin[36] (Sigma-Aldrich #P4394) was reconstituted to 100 mM in DMSO and incubated at 37ºC for 3 days to prepare a stock solution, which was then stored in aliquots at −20ºC. Cell pellets were resuspended in 1 mL PBS containing 0.5 μM cisplatin, gently vortexed, incubated 5 minutes at room temperature, quenched with 3 mL CCM, pelleted, and resuspended in 1 mL CCM. Cells were fixed by adding 16% paraformaldehyde (PFA; Electron Microscopy Sciences, Hatfield, PA, USA) to a final concentration of 1.6%, gently vortexed, incubated 10 minutes at room temperature, and washed twice with cell staining media (CSM; PBS with 0.5% BSA, 0.02% sodium azide) to remove residual PFA. All centrifuging steps for fixed cells were done for 5 minutes at 600 g, 4ºC. Cell pellets were optionally stored at −80°C.

With the exception of titrations, samples were palladium-barcoded and pooled as described[37] to improve staining consistency. Fc receptor blocking was performed with

Human TruStain FcX (Biolegend #422302) following manufacturer's instructions to prevent non-specific antibody binding. Antibodies against surface antigens were pooled into a master mix in CSM yielding 50 μL (350 μL if barcoded) final reaction volumes per sample and filtered through a 0.1 μm filter (Millipore #UFC30VV00, Billerica, MA, USA) for 5 minutes at 1,000 g to remove antibody aggregates. Antibody master mix was then added to each sample, resuspended, and cells were incubated 30 minutes at room temperature. Mass cytometry antibody panels are listed in Supplementary Data 1-5. With the exception of antibodies purchased from Fluidigm (South San Francisco, CA, USA), all mass cytometry antibodies that were conjugated to reporter metal isotopes in-house were titrated to determine optimal staining concentrations prior to incorporating that antibody into a staining panel. Antibodies were conjugated using MaxPar Antibody Conjugation Kit (Fluidigm) and titrated on cells both positive and negative for the target antigen expression to identify concentration yielding the best signal-to-noise ratio. Following the surface stain, cells were washed with CSM, permeabilized with 4°C methanol for 10 minutes on ice, washed twice with CSM, stained with an antibody master mix (prepared as above) against intracellular antigens in 50 μL (350 μL if barcoded) CSM for 30 minutes at room temperature, and washed once with CSM. To stain DNA, cells were incubated in PBS containing 1:5000 ^{191}Ir/^{193}Ir MaxPar Nucleic Acid Intercalator (Fluidigm) and 1.6% PFA for 1-3 days at 4°C. Just prior to analysis, cells were washed once with CSM and twice with filtered double-distilled water, resuspended in normalization beads[38] (EQ Beads, Fluidigm), filtered, and placed on ice. During event acquisition, cells were kept on ice and introduced into the CyTOF 2 (Fluidigm) using Super Sampler (Victorian Airship and Scientific Apparatus, Alamo, CA, USA). In addition to reporter metal isotopes listed in antibody panels (Supplementary Data 1-5), we recorded event length and channels ^{102}Pd, ^{104}Pd, ^{105}Pd, ^{106}Pd, ^{108}Pd, and ^{110}Pd (barcoding); ^{140}Ce, ^{151}Eu, ^{153}Eu, ^{165}Ho, and ^{175}Lu (bead normalization); ^{191}Ir and ^{193}Ir (DNA); ^{195}Pt and ^{196}Pt (dead cells); and ^{138}Ba (to help define single cells). In experiments quantifying IdU incorporation, we also recorded ^{127}I.

In optimization experiments for CFSE detection, we also tested alternative permeabilization methods (no permeabilization, 0.2% saponin, CFSE staining after permeabilization), multiple anti-FITC antibody clones, concentrations, and detection channels (clone FIT-22 conjugated to 172Yb, 0.25-16 μg/mL, Biolegend #408302; pre-conjugated clone FIT-22 on 144Nd, 0.5-8 tests, Fluidigm #3144006B; clone F4/1 conjugated to 172Yb, 0.25-16 μg/mL, Abcam #ab112511, Cambridge, UK; polyclonal antibody conjugated to 172Yb, 1-64 μg/mL, Southern Biotech #6400-01, Birmingham, AL), and extended anti-FITC incubation time (60 instead of 30 minutes) for all clones.

Singe-cell RNA-sequencing of T-cell division states

Cells were collected as described on day 3 of REP. The lot of PBMCs was previously analyzed in order to obtain the exact timing to observe all 3 division states in the same culture. Here, ~10,000 live CFSE$^+$ CD8$^+$ T cells were prospectively isolated from division 0, 1, or 2 and resuspended in 100 μL CCM. Cells were stored on ice and processed the same day on the Chromium platform (10X Genomics, Pleasanton, CA, USA) at the Stanford Functional Genomics Facility for droplet-based 3' single-cell RNA-sequencing per the manufacturer's instructions, with a target of 3,000 cells per sample and a sequencing depth

of >50,000 reads per cell. The sample libraries were combined and ran on a single lane of the HiSeq 4000 platform (Illumina, San Diego, CA, USA).

Flow cytometry

When comparing mass cytometry and flow cytometry data, viability staining was also performed with Fixable Violet Dead Cell Stain (Thermo Fisher Scientific #L34955). Samples were then fixed as described above and separated into two parts for both flow and mass cytometry analysis just prior to storage at −80ºC. Surface staining was performed with anti-CD3ε-APC (clone UCHT1, Biolegend #300412) and anti-CD8α-APC-H7 (clone SK1, BD Biosciences #560273) antibodies. Cells were then resuspended in 250 μL CSM and analyzed on LSRII flow cytometer (BD Biosciences).

Data processing

Mass cytometry data were normalized[38] and debarcoded[37]. Data were transformed using inverse hyperbolic sine (arsinh) with a cofactor of 5 for DNA or protein expression[7], or with a cofactor of 20 for CFSE. Single cells were gated using *Cytobank* software (www.cytobank.org) based on event length and $^{191}Ir/^{193}Ir$ (DNA) content as described by Bendall *et al.*[7] Live non-apoptotic cells were gated based on ^{195}Pt (viability) content[36] and cleaved PARP (cPARP). Hematopoietic cells were selected based on CD45 expression. In initial experiments (antibody panel from Supplementary Data 1), CD45$^+$ cells were further gated to select CD8$^+$ T cells (CD3ε$^+$ CD4$^-$ CD8α$^+$ CD14$^-$ CD19$^-$ CD20$^-$), myeloid dendritic cells (mDCs; CD3ε$^-$ CD11c$^+$ CD14$^-$ CD19$^-$ CD20$^-$ HLA-DR$^+$), or monocytes (CD3ε$^-$ CD14$^+$ CD19$^-$ CD20$^-$). In experiments focused on differentiation of CD8$^+$ T cells (antibody panels from Supplementary Data 2-5), we also excluded events that were CD33$^+$ (myeloid), CD61$^+$ (platelets), CD235$^+$ (erythrocytes), or TCRγδ$^+$ (γδ T cells). Where indicated, CFSE$^+$ cells were selected based on a CFSE$^-$ control from the same day. An example gating strategy is provided in Supplementary Figs. 3a,b.

Flow cytometry data were transformed using arsinh with a cofactor of 150. CD8$^+$ T cells were gated as single live CD3ε$^+$ CD8α$^+$ events.

Single-cell RNA-sequencing reads were aligned to the Genome Reference Consortium Human Build 38 (GRCh38), normalized for batch effects, and filtered for cell events using the *Cell Ranger* software (10X Genomics). A total of 4,060 cells were sequenced to an average of 52,040 post-normalization reads per cell capturing a median of 18,770 unique molecular identifier (UMI) counts per cell mapping to 3,544 unique genes per cell. The cell-gene matrix was further processed using the *Cell Ranger R Kit* software (10X Genomics) as described by Zheng *et al.*[39] Briefly, we first selected genes with ≥l UMI counts in any given cell (19,222 genes). UMI counts were then normalized to UMI sums for each cell and multiplied by a median UMI count across cells. Next, the data were transformed by taking a natural logarithm of the resulting data matrix. Where indicated, we selected 1,000 most variably expressed genes based on normalized dispersion[39].

Division ID assignment

Single-cell data for CFSE^{+} CD8^{+} T cells were processed using *R* (www.r-project.org) and *Bioconductor* (www.bioconductor.org) software. To assign division IDs to cells in a given sample, we identified division peaks in log2-transformed CFSE ion count or fluorescence data using local regression. Centroid of division 0 peak and peak s.d. were estimated based on non-proliferating control cells collected at the same time. Remaining division IDs were assigned to all cells where assignment confidence was ≥80% based on normal distribution modeling (or division −1 if not assigned). Top and bottom CFSE intensity cutoffs were set at 2x s.d. above division 0 and 2x s.d. below the maximum division, respectively. A modified FCS file with "Division" column appended to original data was then exported for downstream analysis. Fig. 2b shows a summary of the division ID assignment process.

Force-directed layout

To create force-directed graphs, we used *Vortex* software[16] that implements *ForceAtlas2* engine[15, 16]. Here, we extended *Vortex* to only allowing edge connections either between subsequent timepoints (as in the *FLOW-MAP* algorithm[17]), or between subsequent divisions. Data were sampled as indicated prior to graph construction. Cell dissimilarity, a basis for repulsive forces, was calculated based on angular (cosine) distance in indicated dimensions. Edges, a basis for spring-like attractive forces, connected each cell to its 10 nearest neighbors in the original high-dimensional space, which also had to be within consecutive (−1, 0, +1) division states. See Figs. 4a and Fig. 3a for a summary of this process.

Diffusion maps

Diffusion maps embed single-cell data into diffusion components through a non-linear transformation[18, 40]. To perform the embedding, a matrix of diffusion distances is computed among all cells using mathematics of heat diffusion and random walk Markov chains. This matrix is then applied to calculate DPT, a metric based on the transition probability of a diffusion process. To embed data into diffusion components and to calculate DPT, we applied *destiny*[40] implementation of diffusion maps in *R*, which enables identification of up to two endpoints of a differentiation process. Diffusion maps were constructed using angular distance metric and the same markers as in force-directed graphs. Diffusion components, DPT values, division IDs, and time (days) were appended to the data, enabling visualization of these parameters in force-directed graphs using *Vortex*. Where indicated, DPT values for different treatment conditions were normalized to 0-1 range for visualization purposes.

Statistical analysis

Statistical analysis was performed using *R* statistical software (www.r-project.org). To assess CFSE correlation between identical samples analyzed by flow and mass cytometry, we calculated Spearman's rank correlation coefficient using log10-transformed medians for each division ID, or using the percentage of cells assigned the same division ID. When no comparison to flow cytometry was made, we calculated Spearman's rank correlation coefficient using arsinh-transformed mass cytometry data. In each case, *P*-values were calculated using correlation test. We tested normality assumption using Shapiro-Wilk test.

As the normality assumption was not met in statistical tests on single-cell data performed here, we applied unpaired two-tailed Wilcoxon Mann-Whitney U test to assess statistical significance between two groups. When more than two groups were compared, we first used Kruskal-Wallis H test (one-way analysis of variance on ranks) to check whether there are differences among treatment groups, followed by unpaired two-tailed Wilcoxon-Mann Whitney test applied to each treatment pair, and Bonferroni correction to correct for multiple hypothesis testing. To assess evidence for a decrease in mean phenotypic diversity with division across experiments, we used *lme4*[41] implementation of linear mixed-effects models in *R*.

We used lasso[19, 42, 43] to identify markers associated with DPT. We allocated 80% of cells into training set and 20% of cells into test set using random sampling. To construct a lasso model, we used *glmnet*[42] implementation of lasso in *R*, including a built-in cross-validation function to tune the L_1 regularization parameter lambda. We then used all training data to construct the final model, and applied that model to the test data to assess performance.

Data availability

Single-cell data can be accessed on *GitHub* (https://github.com/BendallLab/division-history). Singe-cell RNA-sequencing data are also available on *Gene Expression Omnibus* (https://www.ncbi.nlm.nih.gov/geo; GEO accession: GSE119139).

Code availability

An extended version of the Java-based *Vortex* software[16] and documentation can be accessed at https://github.com/nolanlab/vortex.

Supplementary Material

Refer to Web version on PubMed Central for supplementary material.

Acknowledgements

References

1. Chang JT et al. Asymmetric T lymphocyte division in the initiation of adaptive immune responses. Science 315, 1687–1691 (2007). [PubMed: 17332376]

2. Gerlach C et al. Heterogeneous differentiation patterns of individual CD8+ T cells. Science 340, 635–639 (2013). [PubMed: 23493421]

3. Tubo NJ et al. Most microbe-specific naive CD4(+) T cells produce memory cells during infection. Science 351, 511–514 (2016). [PubMed: 26823430]

4. Reiner SL & Adams WC Lymphocyte fate specification as a deterministic but highly plastic process. Nature reviews. Immunology 14, 699–704 (2014).

5. Woodworth MB, Girskis KM & Walsh CA Building a lineage from single cells: genetic techniques for cell lineage tracking. Nature reviews. Genetics 18, 230–244 (2017).

6. Quah BJ & Parish CR New and improved methods for measuring lymphocyte proliferation in vitro and in vivo using CFSE-like fluorescent dyes. Journal of immunological methods 379, 1–14 (2012). [PubMed: 22370428]

7. Bendall SC et al. Single-cell mass cytometry of differential immune and drug responses across a human hematopoietic continuum. Science 332, 687–696 (2011). [PubMed: 21551058]

8. Lyons AB & Parish CR Determination of lymphocyte division by flow cytometry. Journal of immunological methods 171, 131–137 (1994). [PubMed: 8176234]

9. Quah BJ, Lyons AB & Parish CR The use of CFSE-like dyes for measuring lymphocyte proliferation: experimental considerations and biological variables. Mathematical Modelling of Natural Phenomena 7, 53–64 (2012).

10. Li Y & Kurlander RJ Comparison of anti-CD3 and anti-CD28-coated beads with soluble anti-CD3 for expanding human T cells: differing impact on CD8 T cell phenotype and responsiveness to restimulation. Journal of translational medicine 8, 104 (2010). [PubMed: 20977748]

11. Apetoh L et al. Consensus nomenclature for CD8+ T cell phenotypes in cancer. Oncoimmunology 4, e998538 (2015). [PubMed: 26137416]

12. Gattinoni L, Speiser DE, Lichterfeld M & Bonini C T memory stem cells in health and disease. Nature medicine 23, 18–27 (2017).

13. Rosenberg SA & Restifo NP Adoptive cell transfer as personalized immunotherapy for human cancer. Science 348, 62–68 (2015). [PubMed: 25838374]

14. Nish SA et al. CD4+ T cell effector commitment coupled to self-renewal by asymmetric cell divisions. The Journal of experimental medicine 214, 39–47 (2017). [PubMed: 27923906]

15. Jacomy M, Venturini T, Heymann S & Bastian M ForceAtlas2, a continuous graph layout algorithm for handy network visualization designed for the Gephi software. PloS one 9, e98679 (2014). [PubMed: 24914678]

16. Samusik N, Good Z, Spitzer MH, Davis KL & Nolan GP Automated mapping of phenotype space with single-cell data. Nature methods 13, 493–496 (2016). [PubMed: 27183440]

17. Zunder ER, Lujan E, Goltsev Y, Wernig M & Nolan GP A continuous molecular roadmap to iPSC reprogramming through progression analysis of single-cell mass cytometry. Cell stem cell 16, 323–337 (2015). [PubMed: 25748935]

18. Coifman RR et al. Geometric diffusions as a tool for harmonic analysis and structure definition of data: diffusion maps. Proceedings of the National Academy of Sciences of the United States of America 102, 7426–7431 (2005). [PubMed: 15899970]

19. Tibshirani R Regression shrinkage and selection via the lasso. Journal of the Royal Statistical Society, Series B, 267–288 (1996).

20. Xu L, Zhang Y, Luo G & Li Y The roles of stem cell memory T cells in hematological malignancies. J Hematol Oncol 8, 113 (2015). [PubMed: 26462561]

21. Sabatino M et al. Generation of clinical-grade CD19-specific CAR-modified CD8+ memory stem cells for the treatment of human B-cell malignancies. Blood 128, 519–528 (2016). [PubMed: 27226436]

22. Dubovsky JA et al. Ibrutinib is an irreversible molecular inhibitor of ITK driving a Th1-selective pressure in T lymphocytes. Blood 122, 2539–2549 (2013). [PubMed: 23886836]

23. Begum J et al. A method for evaluating the use of fluorescent dyes to track proliferation in cell lines by dye dilution. Cytometry. Part A : the journal of the International Society for Analytical Cytology 83, 1085–1095 (2013). [PubMed: 24166880]

24. Marchingo JM et al. T cell signaling. Antigen affinity, costimulation, and cytokine inputs sum linearly to amplify T cell expansion. Science 346, 1123–1127 (2014). [PubMed: 25430770]

25. Salter AI et al. Phosphoproteomic analysis of chimeric antigen receptor signaling reveals kinetic and quantitative differences that affect cell function. Science signaling 11 (2018).

26. Kalia V et al. Prolonged interleukin-2Ralpha expression on virus-specific CD8+ T cells favors terminal-effector differentiation in vivo. Immunity 32, 91–103 (2010). [PubMed: 20096608]

27. Long M et al. Ibrutinib treatment improves T cell number and function in CLL patients. The Journal of clinical investigation 127, 3052–3064 (2017). [PubMed: 28714866]

28. Turtle CJ et al. Durable Molecular Remissions in Chronic Lymphocytic Leukemia Treated With CD19-Specific Chimeric Antigen Receptor-Modified T Cells After Failure of Ibrutinib. Journal of clinical oncology : official journal of the American Society of Clinical Oncology 35, 3010–3020 (2017). [PubMed: 28715249]

29. Fraietta JA et al. Ibrutinib enhances chimeric antigen receptor T-cell engraftment and efficacy in leukemia. Blood 127, 1117–1127 (2016). [PubMed: 26813675]

30. Gill S et al. CD19 CAR-T cells combined with ibrutinib to induce complete remission in CLL. Journal of clinical oncology : official journal of the American Society of Clinical Oncology 35, suppl; abstr 7509 (2017).

31. Quah BJ & Parish CR The use of carboxyfluorescein diacetate succinimidyl ester (CFSE) to monitor lymphocyte proliferation. Journal of visualized experiments : JoVE (2010).

32. Advani RH et al. Bruton tyrosine kinase inhibitor ibrutinib (PCI-32765) has significant activity in patients with relapsed/refractory B-cell malignancies. Journal of clinical oncology : official journal of the American Society of Clinical Oncology 31, 88–94 (2013). [PubMed: 23045577]

33. Marostica E et al. Population pharmacokinetic model of ibrutinib, a Bruton tyrosine kinase inhibitor, in patients with B cell malignancies. Cancer chemotherapy and pharmacology 75, 111–121 (2015). [PubMed: 25381051]

34. Araki K et al. mTOR regulates memory CD8 T-cell differentiation. Nature 460, 108–112 (2009). [PubMed: 19543266]

35. Stenton SB, Partovi N & Ensom MH Sirolimus: the evidence for clinical pharmacokinetic monitoring. Clinical pharmacokinetics 44, 769–786 (2005). [PubMed: 16029064]

36. Fienberg HG, Simonds EF, Fantl WJ, Nolan GP & Bodenmiller B A platinum-based covalent viability reagent for single-cell mass cytometry. Cytometry. Part A : the journal of the International Society for Analytical Cytology 81, 467–475 (2012). [PubMed: 22577098]

37. Zunder ER et al. Palladium-based mass tag cell barcoding with a doublet-filtering scheme and single-cell deconvolution algorithm. Nature protocols 10, 316–333 (2015). [PubMed: 25612231]

38. Finck R et al. Normalization of mass cytometry data with bead standards. Cytometry. Part A : the journal of the International Society for Analytical Cytology 83, 483–494 (2013). [PubMed: 23512433]

39. Zheng GX et al. Massively parallel digital transcriptional profiling of single cells. Nature communications 8, 14049 (2017).

40. Angerer P et al. destiny: diffusion maps for large-scale single-cell data in R. Bioinformatics 32, 1241–1243 (2016). [PubMed: 26668002]

41. Bates D, Machler M, Bolker BM & Walker SC Fitting Linear Mixed-Effects Models Using lme4. Journal of Statistical Software 67, 1–48 (2015).

42. Friedman J, Hastie T & Tibshirani R Regularization Paths for Generalized Linear Models via Coordinate Descent. J Stat Softw 33, 1–22 (2010). [PubMed: 20808728]

43. James G, Witten D, Hastie T & Tibshirani R An Introduction to Statistical Learning with Applications in R, Edn. 6th (Springer Texts in Statistics, 2015).
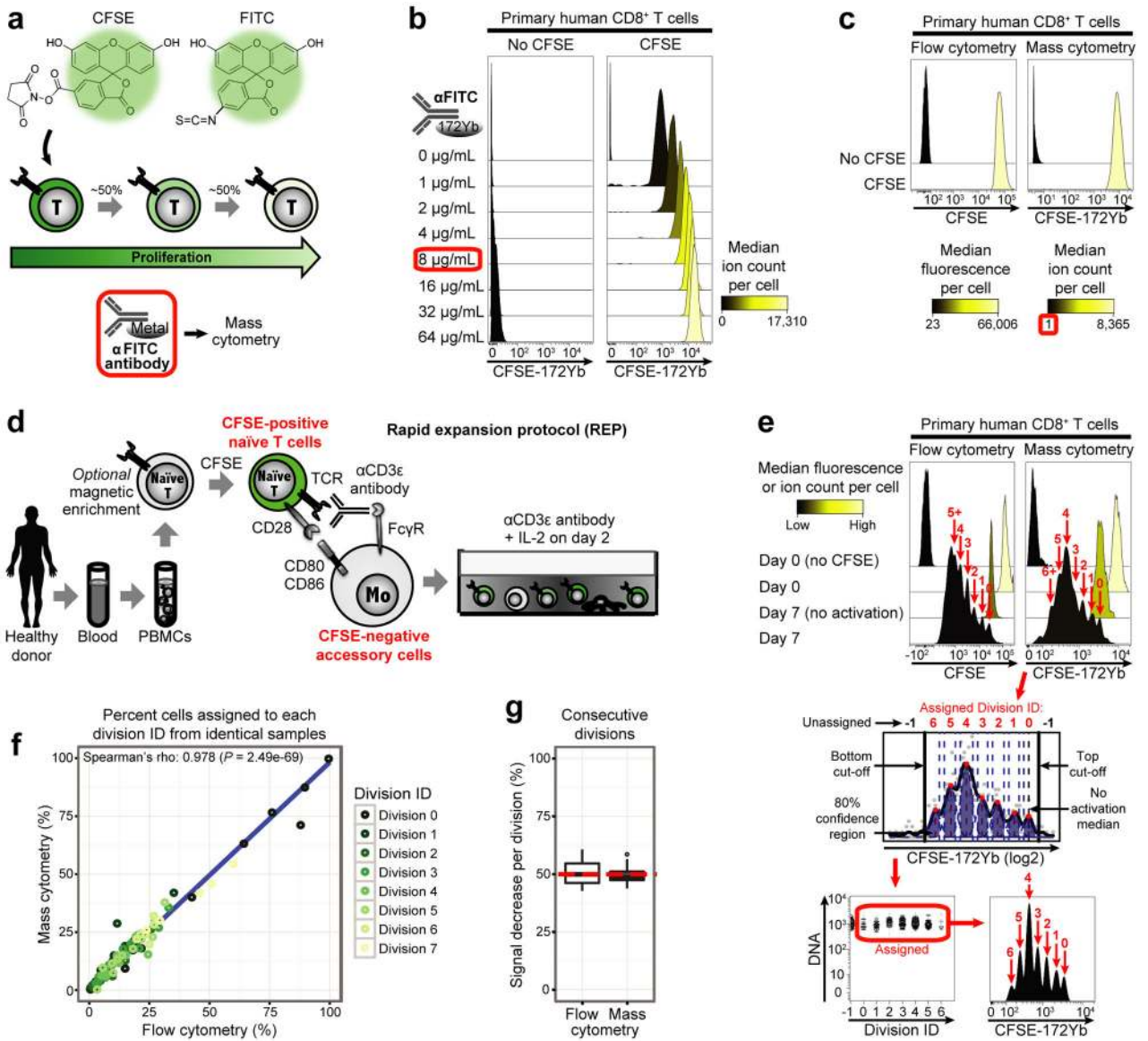
Figure 1: CFSE can be used to obtain proliferative history and trace cells of interest in complex cultures by mass cytometry.

(a) A strategy for adapting CFSE dye dilution assay to mass cytometry. Since both CFSE and FITC are derivatives of fluorescein, CFSE can be quantified by mass cytometry using intracellular staining with an anti-FITC antibody conjugated to a reporter metal isotope. With each division, daughter cells inherit ~50% of CFSE, providing a proxy for estimating the number of cell divisions (proliferative history). **(b)** Mass cytometry titration of a polyclonal anti-FITC-^{172}Yb antibody on human CD8$^+$ T cells, with the optimal concentration highlighted (red box). **(c)** Equivalent CFSE signal obtained from human CD8$^+$ T cells analyzed in parallel by flow cytometry and mass cytometry, with the near-zero anti-FITC-^{172}Yb antibody background highlighted (red box). **(d)** Experimental outline for tracing proliferative history of naïve CD8$^+$ T cells in REP as a model system. CFSE-labeled naïve human T lymphocytes are induced to proliferate by CFSE-negative accessory cells,

including monocytes (Mo), that present an anti-CD3ε antibody via Fcγ receptors (FcγRs) and express co-stimulatory molecules. Interleukin-2 (IL-2) is added after 48 hours. **(e)** Proliferative history of CD8$^+$ T cells was similar when measured directly by flow cytometry, or indirectly using a ^{172}Yb-labeled anti-FITC antibody by mass cytometry. A division ID (red arrows) was assigned to each cell falling into the ≥80% confidence region (blue), or division ID: −1 otherwise. Division IDs were added to the original file, enabling downstream analysis in software of choice, such as *Cytobank*. **(f)** Spearman correlation analysis comparing percentage of cells falling into each division state in samples analyzed in parallel by flow cytometry and mass cytometry (n = 26 time-series samples from 6 REP cultures). **(g)** CFSE signal reduction per division was calculated based on geometric means from cells in (f). Boxplots show quartiles with a band at median, whiskers indicating 1.5 interquartile range (IQR), and outliers shown separately. A red dashed line indicates the expected 50% reduction. The antibody was titrated once; results in (c,e-g) are from 1 experiment representative of 3 experiments. Results in (b-c) and (e-g) were obtained using antibody panels in Supplementary Data 1 and Supplementary Data 2, respectively.
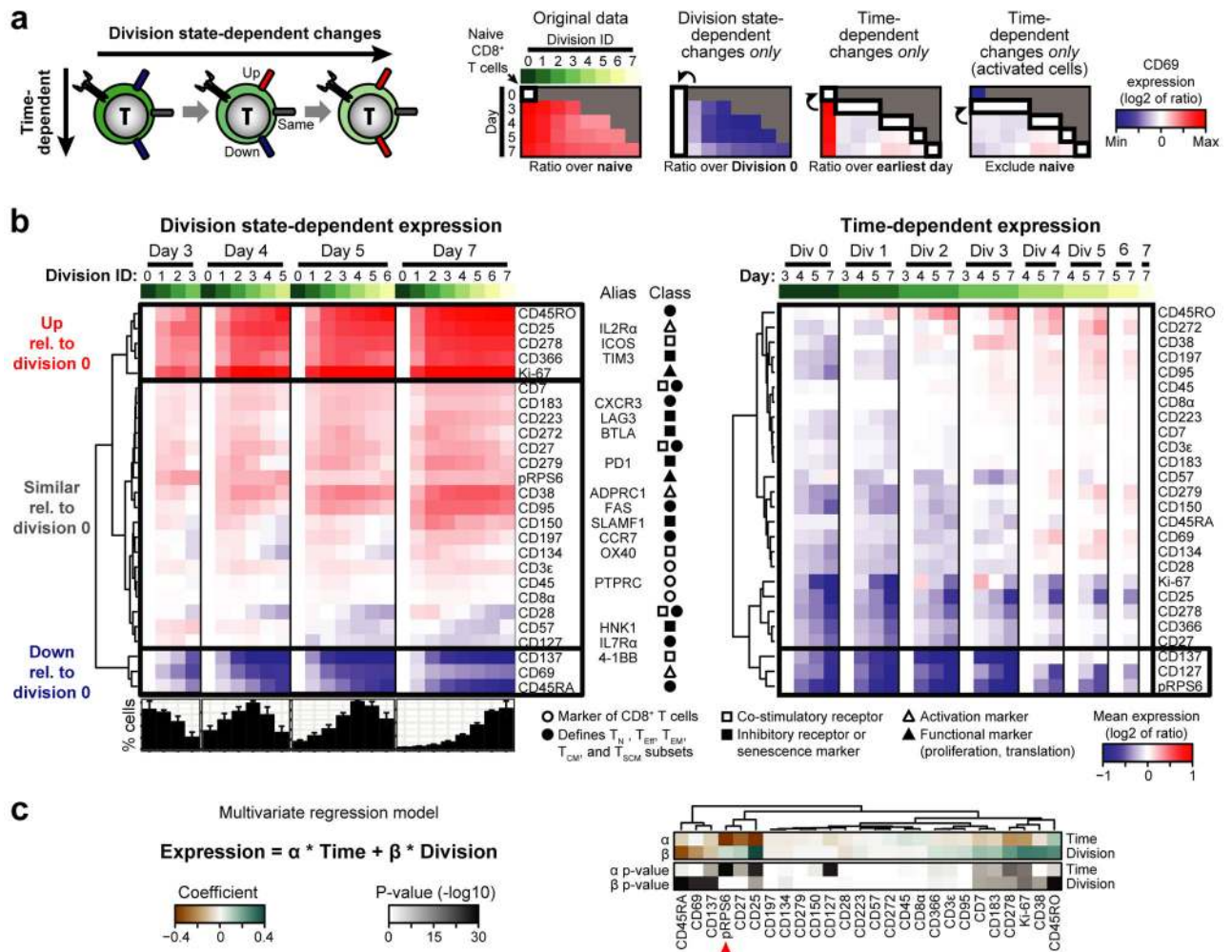
Figure 2: Uncoupling time and division state in expansion of naïve CD8$^+$ T cells shows that early differentiation is linked to both time and proliferation.

(a-c) Naïve CFSE-labeled T cells were expanded using REP, collected on days 0, 3, 4, 5, and 7 (n = 26 time-series samples from 6 cultures), analyzed by mass cytometry using an antibody panel in Supplementary Data 2, and gated on live non-apoptotic CFSE$^+$ CD8$^+$ T cells. **(a)** A normalization scheme to examine time- and division state-dependent changes as orthogonal dimensions. To focus on *division state-dependent* changes only, expression is divided by division 0 at the same timepoint. To focus on *time-dependent* changes only, expression is divided by the earliest timepoint with the same division ID (except day 0 to focus on activated cells). CD69 is shown as an example. **(b)** Changes in average *division state-dependent* expression (left) or *time-dependent* expression (right) of 23 markers (plus CD3ε, CD8α, CD45 that were also used for gating) in CFSE-traced CD8$^+$ T cells. See Supplementary Data 6 for additional information on each marker. Bar graphs show division state distribution on each day as mean ± s.e.m. **(c)** A multivariate linear regression model to assess relative effects of time and division state on protein expression. Model coefficients and their *P*-values are shown as a heatmap for each marker. Results in (a-c) are from 1

experiment representative of 3 experiments. T_N, naïve T cells; T_{CM}, central memory T cells; T_{EM}, effector memory T cells; T_{SCM}, stem cell memory T cells.
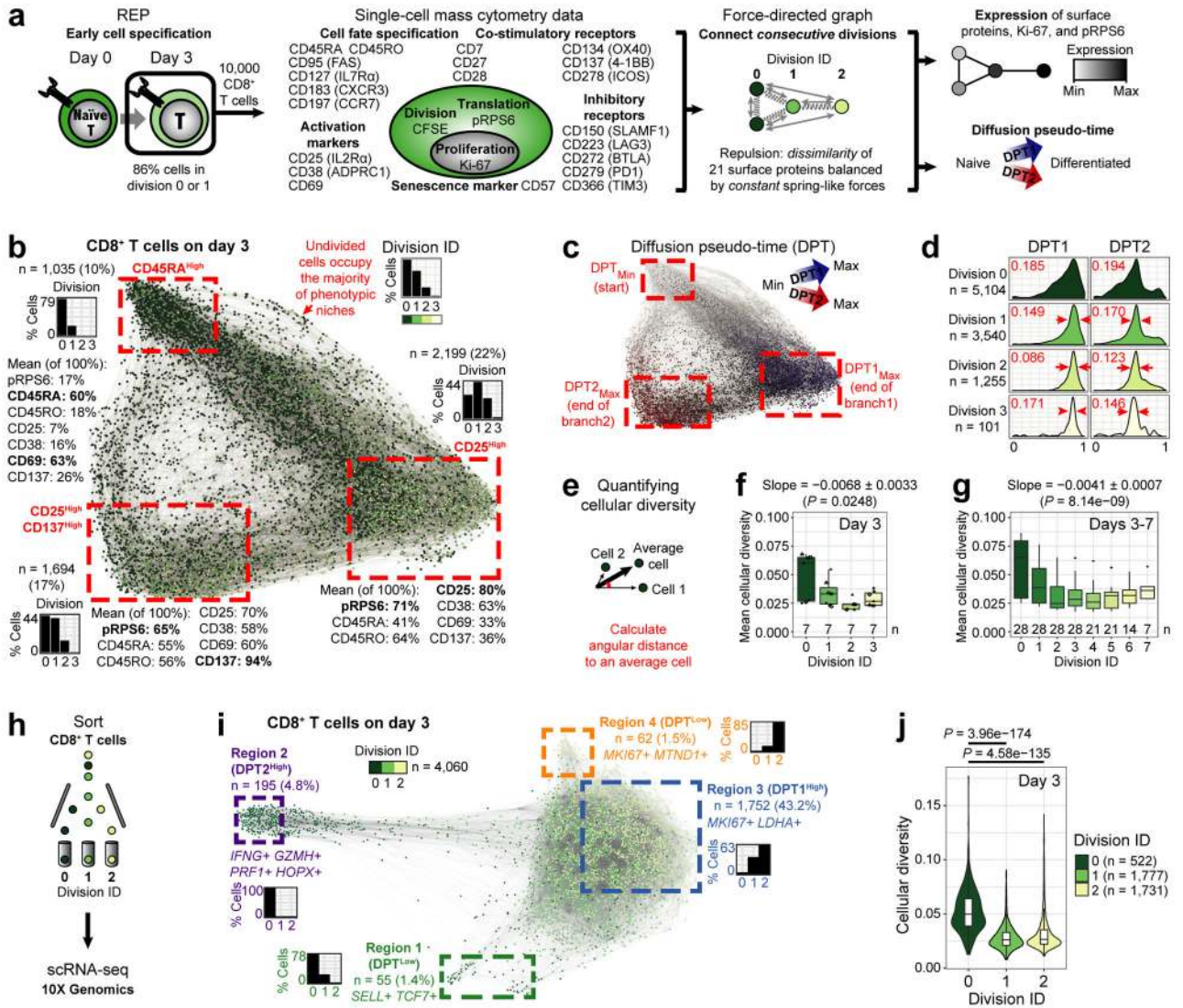
Figure 3: Undivided cells display the highest phenotypic diversity in early naïve T-cell differentiation.

(a) Force-directed graph was constructed with 10,000 CFSE+ CD8+ T cells from day 3 of REP analyzed by mass cytometry using an antibody panel in Supplementary Data 2. Cells repel based on expression of 21 surface proteins. Edges connect *only* cells in neighboring division states. (b) Division IDs overlaid onto phenotypic map from (a). Marker expression was scaled to 0-100% prior to calculating mean expression within each region. (c) DPT calculated using 21 surface proteins and overlaid onto the graph from (b). Colors were scaled to emphasize separation of DPT1 and DPT2. (d) DPT histograms separated by division. Red arrows indicate the narrowing in DPT s.d. within each division. Results in (b-d) are from 1 donor representative of 5 donors. (e) High-dimensional phenotypic diversity was estimated as a cosine distance to an average cell within each division state. (f) Mean phenotypic diversity of CFSE+ CD8+ T cells on day 3 (n = 7 REP cultures). (g) Mean phenotypic diversity on days 3, 4, 5, and 7 (n = 28 time-series samples from n = 7 REP cultures). Phenotypic diversity in (f-g) was calculated as described in (e) using 18 common

proteins. Boxplots show quartiles with a band at median, whiskers indicating 1.5 IQR, and outliers shown separately. To assess evidence for a decrease in phenotypic diversity with division, we used linear mixed-effects models; slope ± s.e. and *P*-values are shown above each plot. **(h-j)** 10,000 CFSE$^+$ CD8$^+$ T cells from divisions 0, 1, and 2 were sorted for droplet-based scRNA-seq on day 3 of REP. Out of 19,222 genes detected in n = 4,060 cells (division 0: n = 522; division 1: n = 1,777; division 2: n = 1,731 sequenced in 1 experiment), we selected 1,000 most variably expressed genes for analysis in (i-j). **(i)** A force-directed graph constructed as in (a). **(h)** Phenotypic diversity calculated as in (e). Violin plots show a kernel density estimate with a boxplot, which contains quartiles with a band at median and whiskers indicating 1.5 IQR. Kruskal-Wallis *H* test (one-way ANOVA on ranks): *P* = 1.58e −177; two-sided Wilcoxon Mann-Whitney (WMW) *U* test comparing division 0 *vs.* division 1: *P* = 3.96e−174, comparing division 0 *vs.* division 2: *P* = 4.58e−135. WMW *P*-values were corrected for multiple hypotheses testing using Bonferroni correction.
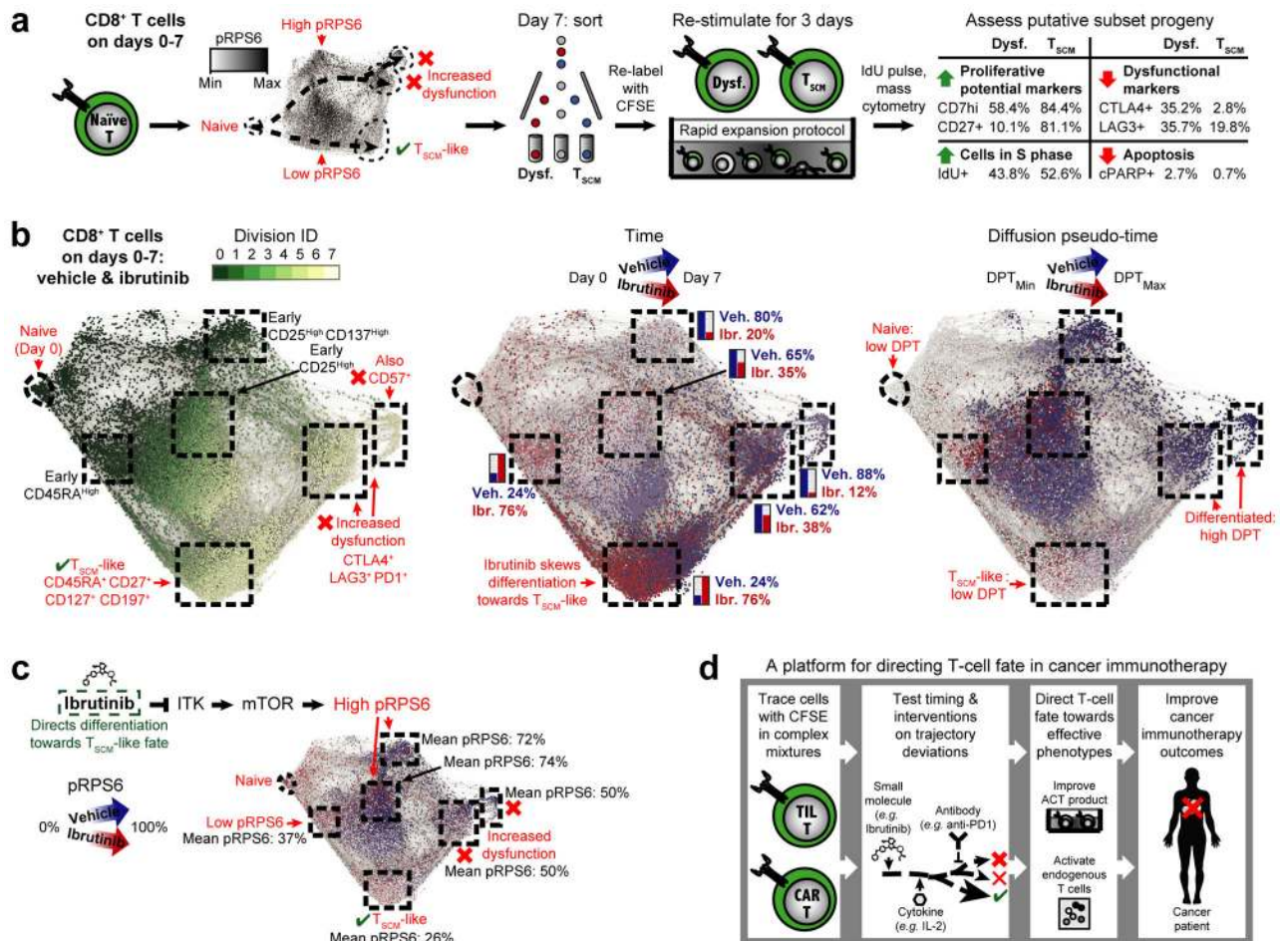
Figure 4: Ibrutinib directs naive T-cell differentiation towards T$_{SCM}$-like state.

(a) Naïve CFSE$^+$ CD8$^+$ T-cell differentiation in REP converges onto T$_{SCM}$-like cells (pRPS6^{Low} path) and dysfunctional-phenotype cells (pRPS6^{High} path) by day 7 (Supplementary Figs. 13-14), with properties assessed in re-stimulation experiments (Supplementary Fig. 16) and summarized on the right. **(b)** REP cultures were treated with either vehicle (DMSO) or ibrutinib, collected on days 0, 3, 4, 5, and 7, and assessed by mass cytometry using an antibody panel in Supplementary Data 3. CFSE$^+$ CD8$^+$ T cells were pooled into a force-directed graph constructed using 27 surface proteins, with edges connecting cells only in neighboring divisions. Naïve T-cell differentiation can be observed across divisions (left), time (center), or DPT (right) when overlaid onto the graph. DPT was calculated using 27 surface proteins (separately for each treatment condition), and then scaled from 0 to 1 to improve visibility (*i.e.* DPT values for ibrutinib appear inflated on average 2.2x). Graph regions were defined using individual marker expression (Supplementary Fig. 15). Results were nearly identical when only proteins from the original panel (Supplementary Data 2) were used instead of the extended panel (Supplementary Data 3). **(c)** pRPS6 overlaid onto the graph from (b) and colored by treatment condition. A signaling pathway links ibrutinib to pRPS6. Results in (b-c) are from 1 donor representative of 3 donors from 2 experiments. **(d)** A summary of potential cancer immunotherapy applications of the platform presented here. Tracing fate of CFSE$^+$ TILs or CAR T cells

across time and divisions in complex cell mixtures may be useful for rationally selecting timing and interventions for guiding T-cell fate during *ex vivo* expansion for ACT. These insights may be later used for designing better drugs to improve T-cell function *in situ*.